Multi-Model Machine Learning Analysis of Urban Temperature Trends: A Comparative Study on Climate Change Impacts in U.S. Cities of Midwest KANI Region

Mirza Md Tasnim Mukarram[1*], Quazi Umme Rukiya[2], Marc Linderman[3]

[1]School of Earth, Environment and Sustainability University of IOWA, Iowa city, Iowa,IA-52242, USA, Email: mtasnimmukarram@uiowa.edu, ORCID ID: 0000-0001-5113-3813
[2]School of Earth, Environment and Sustainability, University of IOWA, Iowa city, Iowa,IA-52242, USA, Email: qrukiya@uiowa.edu , ORCID ID: 0009-0001-1509-034X
[3]School of Earth, Environment and Sustainability, University of IOWA, Iowa city, Iowa,IA-52242, USA, Email: marc-linderman@uiowa.edu ORCID ID: 0000-0003-3264-9536

[1*](Corresponding author), PhD Student, School of Earth, Environment and Sustainability University of IOWA, Iowa city, Iowa,IA-52242, USA, Email: mtasnimmukarram@uiowa.edu, ORCID ID: 0000-0001-5113-3813

Abstract

Urban temperature prediction is critical for regional climate planning, environmental monitoring and thermal hazard mitigation. This study employs a multi-model supervised machine learning framework to predict and forecast daily urban air temperatures and evaluate model performance across key counties in the U.S Midwest KANI region: Polk (IA), Pulaski (AR), Lancaster (NE), and Johnson (KS), encompassing 38 urban centres. Using ERA5 Land reanalysis data (2000-2024) from cloud-based Google Earth Engine platform, this study compares six regression-based ML models: Linear Regression, Random Forest, XGBoost, Support Vector Regression (SVR), K-Nearest Neighbors (KNN), and Decision Tree to evaluate their predictive efficacy in forecasting urban temperature changes. Using 288 months of temperature data across 4 major economically important counties, we trained and evaluated each model using R^2, RMSE, and MAE metrics. Ensemble tree-based models XGBoost and Random Forest achieved the strongest performance in daily temperature forecasting across all counties from 2020 to 2024, with R^2 values around 0.91, RMSE between 2.60°C and 3.54°C, and MAE as low as 1.88°C. These models successfully captured seasonal dynamics, with forecasted daily temperatures ranging from –15°C during winter extremes to over 31°C in summer peaks. A Friedman test followed by Nemenyi post-hoc analysis confirmed that Decision Tree significantly underperformed compared to XGBoost ($p = 0.04$) and SVR ($p = 0.03$), while XGBoost, RF, SVR, and KNN formed a statistically indistinguishable high-performance cluster ($p > 0.05$). Linear Regression and Decision Tree were both outside this group, exhibiting poorer accuracy and greater bias, particularly in extreme conditions. These findings emphasize the superior reliability of ensemble methods for operational climate forecasting and highlight the practical forecast range of –15°C to +32°C, enabling precise early warning systems for climate adaptation and heat risk planning across vulnerable counties in the U.S. Midwest.

Keywords: Machine Learning Models, Urban Temperature Prediction, Trend Analysis, Early Warning System, Environmental Modelling

1. Introduction

Climate change is one of the most pressing global challenges of the 21st century (Zhang et al.,2024), with rising temperatures playing a critical role (Uluocak and Bilgili,2024) in driving widespread social, environmental and economic disruptions. Over the past four decades, global surface temperatures have increased at an average rate of 0.032°C per year, while monthly precipitation levels have declined by approximately 0.074 mm (Li et al.,2024; Kumar et al.,2024). In the last decade, temperature variability has become a critical concern in environmental modelling, climate planning (Rakhee et al.,2024), resource management and infrastructure design, especially as societies attempt to adapt to both incremental changes and extreme events. Such trends have placed increasing pressure on urban areas, where climate-induced heat risks are compounded by urban heat island (UHI) effect, a phenomenon that can raise city-center temperatures several degrees above nearby countryside. The UHI not only increases average urban temperatures but also amplifies the intensity and duration of heatwaves in cities, compounding health risks for residents. Impervious surfaces (e.g., concrete and asphalt), along with limited vegetation and high anthropogenic heat emissions, further exacerbate this issue, resulting in elevated temperatures in urban cores compared to surrounding rural areas (Wang et al., 2025; Islam et al.,2024).

Furthermore, heat-related extreme events now rank among the deadliest weather-related hazards (Franzke and Torelló,2020; McDonald et al.,2024), accounting for a significant number of premature deaths annually across both developed and developing nations (Brimicombe et al.,2024). These intersecting challenges highlight the urgency of developing improved forecasting and mitigation strategies tailored to urban environments (Huang et al.,2025) that are not only scalable and interpretable, but also capable of supporting data-driven policymaking and accurately forecasting urban thermal responses to evolving climatic conditions (Uluocak and Bilgili,2024).

Accurate daily temperature prediction supports a range of sectors, from agriculture and water resource management to energy systems, health response planning (Gong et al.,2022; Fister et al.,2023) and the evaluation of climate-related hazards (Elseidi, 2025; Wang et al.,2023). For instance, farmers rely on daily forecasts to plan field activities (Pujahari et al.,2022; Javaid et al.,2023), energy utilities must anticipate temperature-driven demand fluctuations, and city officials use heat predictions to issue warnings for heatwaves (McGregor, 2024; Pascal et al.,2021, Das et al.,2024).

Recent advances in artificial intelligence and machine learning offer promising pathways for improving urban climate forecasting by emphasizing the need for models that are not only accurate but also transparent and reliable for decision-making (Waqar,2024; Taherdoost,2023; Ali et al.,2021). To apply AI in environmental modelling, it is essential to develop models that are precise, transparent, and dependable, in order to earn the trust of stakeholders and comply with policy standards (Camps-Valls et al.,2025). In other words, next-generation climate analytics should strive for a balance between complexity and interpretability (Dawar et al., 2025). While sophisticated non-linear models (e.g., deep learning) can capture complex relationships, their "black box" nature can be a hindrance in policy contexts. Thus, there is a pressing need for modeling frameworks that are both transparent and robust, capable of processing high-resolution datasets while remaining explainable and policy relevant.

In response, this chapter focuses on the U.S. Midwest EPSCoR states specifically the KANI region: Polk (IA), Pulaski (AR), Lancaster (NE), and Johnson (KS), covering 38 cities of varying population and infrastructure profiles. Using daily 2m air temperature data from the

ERA5-Land reanalysis product (2000–2024) in Google Earth Engine, this study develops a multi-model supervised learning framework to forecast urban air temperatures and evaluate model performance. Six regression-based models are examined: Linear Regression, Random Forest, XGBoost, Support Vector Regression, K-Nearest Neighbors, and Decision Tree. Each model is evaluated using R^2, RMSE, and MAE metrics, with forecasts made one day ahead across the historical dataset. To evaluate statistical significance in performance differences, this study will employ the Friedman test followed by Nemenyi post-hoc comparisons. This analytical approach provides insights not only into model accuracy, but also their generalizability and applicability for operational forecasting.

This study demonstrates the value of model interpretability and parsimony, showing that the most complex model is not always the most accurate. This comparative study aims to provide a roadmap for integrating AI/ML techniques into urban temperature prediction. By focusing on the Midwest KANI region, this chapter will demonstrate the potential for data-driven early warning systems in areas that have received less attention in climate research. This study highlights that simpler, transparent models can sometimes rival advanced algorithms in performance, which is encouraging for resource-strapped planning agencies that require reliable and explainable forecasts.

Ultimately, this research aims to support urban policymakers, environmental scientists, climate scientists, and data scientists in harnessing machine learning for improved urban temperature prediction and proactive climate risk management, ensuring that even mid-sized cities in the Midwest are better prepared for the challenges of a warming world. The following sections of this paper will detail the methodology of the multi-model approach, present the comparative results across the four counties, and discuss the implications for urban climate adaptation strategies.

2. Methods & Mathematical Formulae

2.1. Study area

The study area covers the midwestern USA, also introduced as the KANI region in this research. A lot of research work has been conducted state-wise, country-wise, and globally on air temperature. Very few research covers the regional or county-based research works on air temperature trend. In this study, we took four counties, Johnson County, Kansas, Pulaski County, Arkansas, Lancaster County, Nebraska, and Polk County, Iowa, for their significance in highest population and being important as economic zones of the corresponding states. The study area is shown on **Fig. 2.1.**

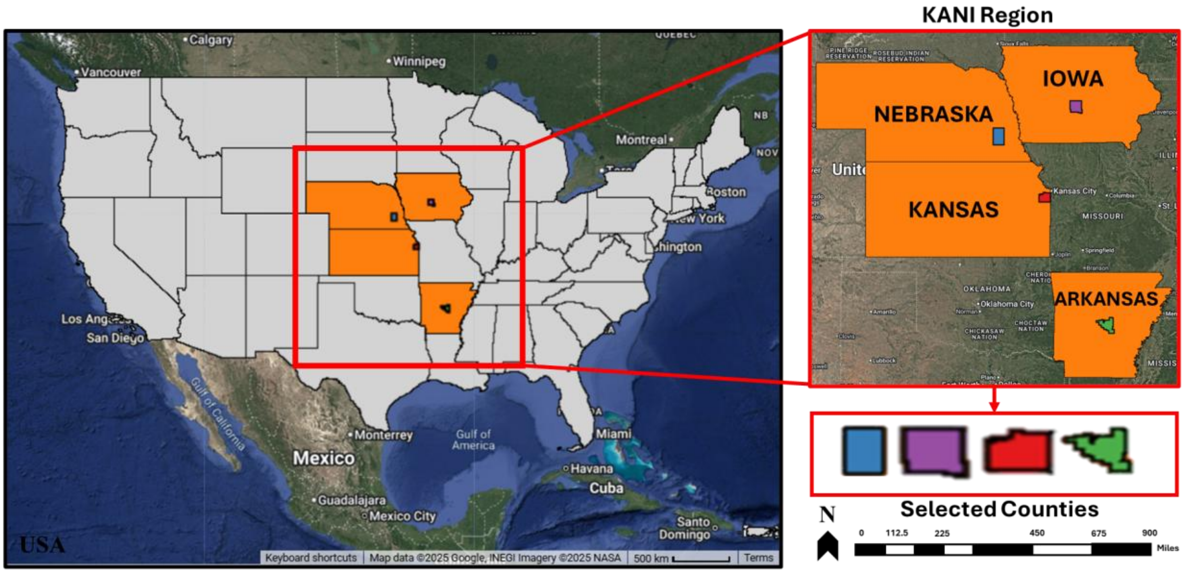

Fig.2.1: Location of the Study Area (Midwest U.S)

2.1.1. Population

One important parameter we considered for selecting the study area is population. From the US Census Bureau, 2023, the highest population counties are selected from each specific state, as air temperature is mostly linked to the human comfort zone and health. In the **Table. 1** the statistics of geography, climate, seasons, and populations of the regions are summarized.

Table 1: Geographic location, climate classification, seasonal descriptions, and population statistics of study area (Midwest KANI Region)

County (State)	**Geographic Coordinates** (USGS,2023)	**Climate Zone**	**Description of Seasons (n=4)** (NOAA,2023)	**Population** (U.S. Census Bureau, 2023)
Johnson (KS)	38.8936° N 94.8075° W	Humid Continental	Spring: Mild & rainy Summer: Hot, humid Fall: Cool & dry Winter: Cold, snow possible	632,276
Pulaski (AR)	34.7387° N 92.2848° W	Humid Subtropical	Spring: Long, stormy Summer: Very hot & humid Fall: Mild & colorful Winter: Short, mild	401,209
Lancaster (NE)	40.7842° N 96.6878° W	Humid Continental	Spring: Warming up with storms Summer: Hot & muggy Fall: Crisp & dry Winter: Snowy, cold	332,857
Polk (IA)	41.6843° N 93.5688° W	Humid Continental	Spring: Cool & wet Summer: Warm & stormy Fall: Sharp temp drops Winter: Long, snowy	516,185

2.1.2. Economy

Another parameter we took while selecting the area of interest is the economy of the counties. The significant economic zones are taken as the study area, where air temperature plays important role. To identify the economically significant counties within the state, we utilized satellite-derived nighttime light data available through GEE, shown in **Fig.2.2.** Nighttime lights, which capture artificial illumination from human settlements, serve as a reliable proxy for economic activity, especially in areas where ground-based economic indicators may be limited or outdated. We accessed annual composites of nighttime light intensity and spatially analysed the distribution across the counties. By comparing the relative brightness levels, we were able to pinpoint regions with consistently higher light emissions, typically corresponding to urban centres, industrial hubs, and areas of dense infrastructure. These counties were then selected as key zones of economic importance for our analysis. Details of the NOAA, VIIRS, US census bureau data used are listed in **Table.2** and **Table.3-**

Table.2: Details of the VIIRS Data

Collection	NOAA/VIIRS/DNB/MONTHLY_V1/VCMCFG
Band	Avg rad = average radiance (light intensity)
Resolution	~500 m
Coverage	Global
Time Period Used	January 1 – December 31, 2023
Operation	Annual mean computed using mean ()

Table.3: Sources of data collection

Dataset ID	**Source**	**Description**	**Use**
TIGER/2018/States	US Census Bureau (TIGER)	U.S. state boundaries	To extract state boundaries
TIGER/2018/Counties	US Census Bureau (TIGER)	U.S. county boundaries	To extract county boundaries
NOAA/VIIRS/DNB/MONTHLY-V1/VCMCFG	NOAA/NASA VIIRS	Monthly average nighttime lights (Avg-rad) from VIIRS DNB	To analyze economic activity via light intensity over Iowa in 2023

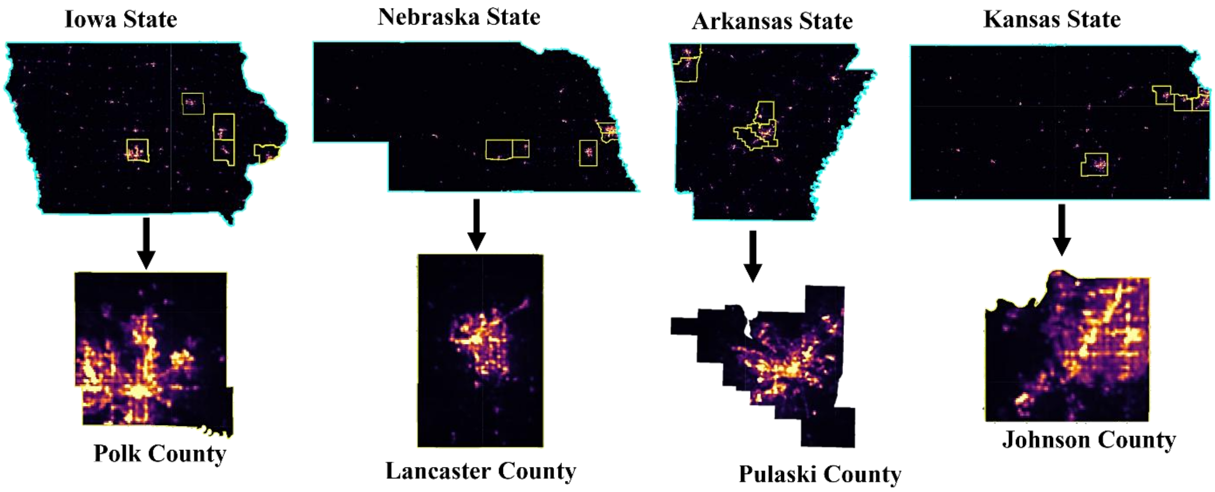

Fig.2.2: Significant economic zone determined by Nighttime light

2.2. Data Acquisition & Pre-processing

After defining the study area, we began data collection and pre-processing by retrieving hourly near-surface air temperature (at 2 meters above ground) from 2000 to 2024 through GEE, described in **Table.4**. This data was obtained from the ERA5-Land reanalysis dataset by the European Centre for Medium-Range Weather Forecasts (ECMWF), which provides consistent, high-resolution hourly global data. ERA5-Land was chosen because it uniquely records hourly air temperature data suitable for long-term regional climate studies. The data was spatially filtered according to county boundaries within our selected states to ensure local relevance. Since air temperature was the sole variable needed at this stage, it was the only one downloaded from GEE in raw form. All datasets were subjected to a comprehensive quality control process using Python workflows designed for large environmental datasets. Initial checks confirmed no missing data, anomalies, or outliers, maintaining data integrity. Once validated, the datasets were formatted for further exploratory and predictive analysis. The overall research workflow is illustrated in **Fig.2.3.**

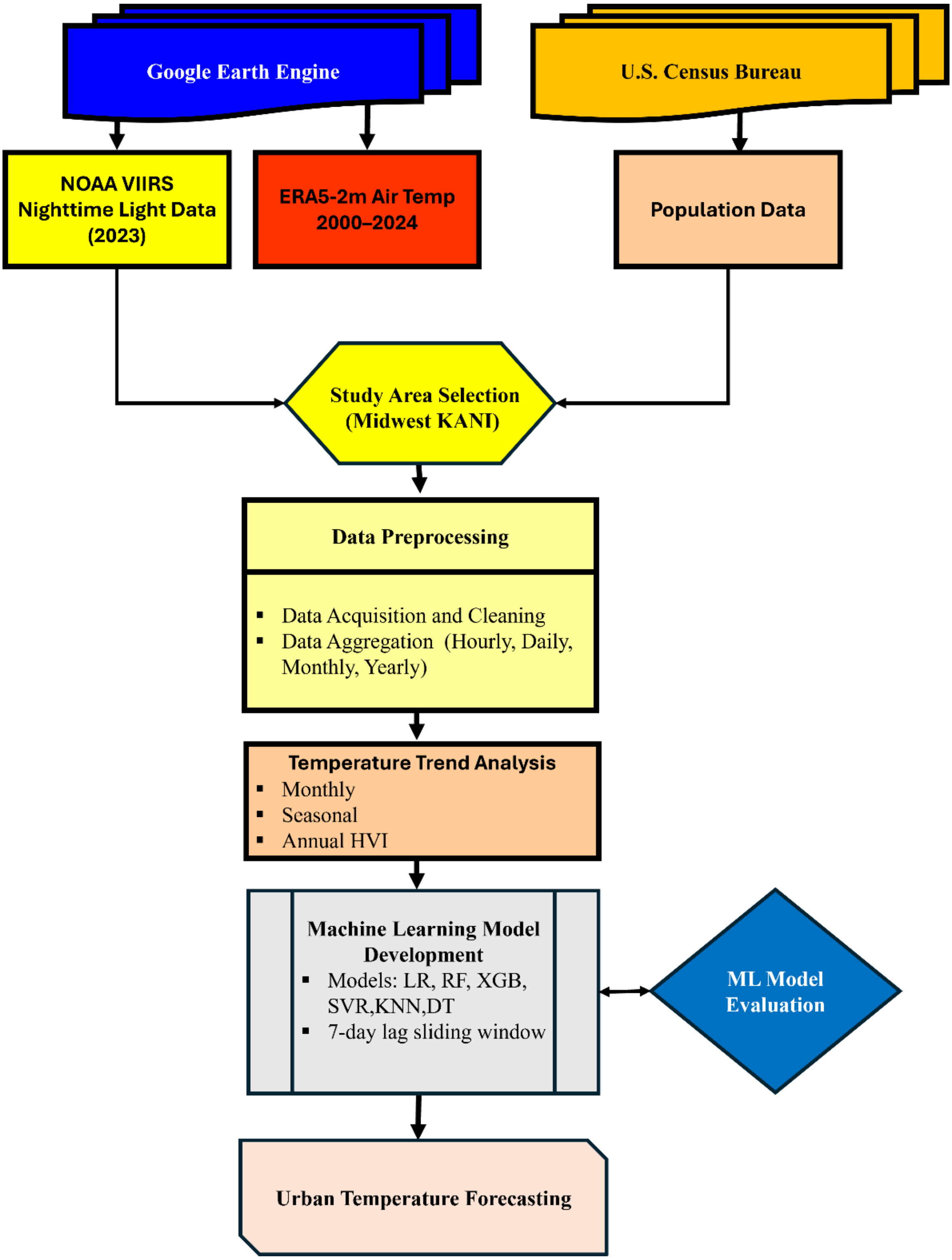

Fig.2.3: Research workflow

Table.4: Details of air temperature data collection

Data type	Time Period	Source
Air temperature (County)	2000-2024	ERA5-Land (ECMWF) via Google Earth Engine
Annual Heat Wave Index (USA)	1895-2021	National Centers for Environmental Information (NCEI)
Heat wave frequency (USA)	1960-2020	CDC National Environmental Public Health Tracking Network
Heat wave duration (USA)	1960-2020	CDC Environmental Tracking
Heat wave season (USA)	1960-2020	Derived from CDC Tracking Network
Heat wave intensity (USA)	1960-2020	CDC Tracking Network

2.3. Trend Analysis

Initial exploratory data analysis (EDA) was performed using raw data from GEE to evaluate regional temporal trends, seasonal variability, and monthly warming patterns. To determine the heat wave index, we extracted daily maximum air temperature data (2 meters above ground) from the ERA5 reanalysis product via Google Earth Engine for the years 2000–2020. The data was processed to identify heat wave events based on a common threshold: periods of at least five consecutive days with temperatures exceeding 25°C. This threshold-based index was calculated annually for each of the four counties to assess the frequency and severity of extreme heat events over time. The results were summarized annually and over five-year intervals for trend analysis and visualization. The following equations 1,2 were applied to derive the HWI using the processed data.

Heat Wave Indicator (binary):

$H_iW_i = 1$ if $t_{max,j} > t_{threshold}$ for $j = i, i+1, ..., i+n\ 1$ .... (1)

$H_iW_i = 0$ otherwise

Where:

$t_{max,j}$ = daily maximum temperature on day j

$t_{threshold}$ = temperature threshold

n = minimum consecutive days

H_iW_i = indicator of a heat wave starting at day i

Heat Wave Index (HWI) for the year:

$HWI_{year} = \sum HW_i$ from i = 1 to N (number of days in the year) .... (2)

In addition to this county-level dataset, we also acquired broader-scale air temperature data across the contiguous United States to support the evaluation of national heatwave trends and contextualize our findings within larger climatological patterns. The EDA was conducted to carry out the following trend analyses described in **Table.5**-

Table.5:

Trends	Boundary	Time frame
1. Annual heatwave events	4 key counties	2000-2020
2. Avg temp (°C)	4 key counties	2000-2024
3. Seasonal temp (°C) (Summer, Fall, Winter, Spring)	4 key counties	2000-2024
4. Monthly avg temp (°C)	4 key counties	2000-2024
5. Annual heat wave index	USA	1895-2021
6. Heat Wave Frequencies	USA	1960s-2020s
7. Heat Wave Duration	USA	1960s-2020s
8. Heat Wave Season	USA	1960s-2020s
9. Heat Wave Intensity	USA	1960s-2020s

2.4. Temperature Prediction Using Machine Learning

2.4.1. Model selection

To predict temperature trends in selected counties across 2000-2024 for determining machine learning model performance, we selected six different machine learning models based on their varying work processes: K-Nearest Neighbours (KNN), Linear Regression, Decision Tree, Support Vector Regression (SVR), Random Forest, and XGBoost. We chose this mix to capture both simple and complex patterns in temperature changes over time. Linear Regression gave a straightforward starting point, while KNN made predictions by comparing past similar conditions. Decision Tree and Random Forest helped us understand more complicated patterns without needing too much fine-tuning. SVR was useful for dealing with more complex data, especially where small details matter. XGBoost, known for its accuracy, handled noisy data well and found hidden relationships between features. By using this variety of models, we aimed to make our temperature forecasts both accurate and reliable across different weather conditions.

2.4.2. Prediction of air temperature

For each county, we calculated the daily mean air temperature using hourly data from the ERA5 dataset from 2000 to 2024. The temperatures, originally in Kelvin, were converted to Celsius, and averaging them by day helped smooth out short-term fluctuations. We ran the models using Google Colab, which made it easier to manage the data and apply machine learning techniques via Python applications. To train the models, we used a 7-day sliding window, meaning the temperatures from the past seven days were used to predict the next day's temperature. This setup helped the models pick up on short-term trends, like steady weather patterns or seasonal shifts. We kept the data in order, training the models on the past 80% and testing them on the most recent 20%, so there was a clear timeline between past and future. Model accuracy was checked using several evaluation methods, and the actual and predicted temperatures were plotted in a single graph for each model to see how well the models performed in each county.

2.4.3.1. Standard evaluation metrics

For assessing the accuracy of the ML models, we are using in this study, we evaluated the performance of the models using the following model evaluation metrics- R^2 to measure goodness-of-fit, RMSE to evaluate prediction error magnitude, and MAE to assess average deviation. The working equations are as follows-

$$R^2 = 1 - \frac{\sum(x_a - x_p)^2}{\sum(x_a - \overline{x_a})^2} \qquad (2.1)$$

$$\text{RMSE} = \sqrt{\frac{1}{n}\sum_{i=1}^{n}(x_a - x_p)^2} \qquad (2.2)$$

$$\text{MAE} = \frac{1}{n}\sum_{i=1}^{n}|x_a - x_p| \qquad (2.3)$$

Where:

x_a = actual value

x_p = predicted value

x_{mean} = mean of actual values

n = number of observations

2.4.3.2. Friedman and Nemenyi Post Hoc test

The Friedman test is a non-parametric statistical method used to detect significant differences in performance among multiple models evaluated across several datasets or tasks. Unlike parametric tests, it does not assume normality, making it suitable for model comparison in machine learning contexts. For k models evaluated on N data splits, the Friedman statistic is:

$$Q = \frac{12N}{k(k+1)}\sum_{j=1}^{k}\left(R_j - \frac{k+1}{2}\right)^2 \qquad (2.4)$$

Where:

Q = Friedman test statistic

N = number of datasets or folds

k = number of models

r̄_j = average rank of model j

The null hypothesis of equal performance is rejected when the associated p-value falls below the conventional α=0.05 threshold that traces back to Fisher's original significance criterion (Abu-Shaira and Shi,2024). When the Friedman test indicates significant differences, the Nemenyi post-hoc test is applied to perform pairwise comparisons between models. This test determines if any performance gap exists between any two models that exceeds a critical difference (CD) threshold, accounting for the number of models and datasets. Together, these methods provide an effective framework for ranking models and identifying statistically better approaches in multi-model evaluation processes.

2.4.3.3. Critical Difference Diagram

The Critical Difference (CD) diagram visualizes the summary of the results of multiple model comparisons after performing the Friedman and Nemenyi tests. It calculates and shows the average ranks of all models on a horizontal axis, connecting models by a line if their rank difference is smaller than the calculated CD value, ensuring no statistically significant difference. CD threshold is exceeded when models are not connected, stated in equation 2.5, and are considered to be performing significantly differently. This diagram provides a simple and visual way to understand complex statistical comparisons and identifies which algorithms perform the best.

$$\mathrm{CD} = q_{\alpha} \cdot \sqrt{\frac{k(k+1)}{6N}} \quad \text{(2.5)}$$

Where:

CD = Critical Difference

q_{α} = critical value from the Studentized range distribution = 0.05

k = number of models

N = number of datasets

Therefore, the summary of all the evaluation methods is listed in the **Table. 6-**

Table. 6: Details of evaluation metrics

Method	**Purpose**	**Threshold**
R^2	Measures model fitness	0-1
RMSE	Magnitude of prediction error quantification	Non-negative (Lower values indicate better model accuracy)
MAE	Average deviation measurement	Lower values indicate better model accuracy
Friedman test	Checks if significant differences exist among multiple models, but does not indicate where those differences lie	p-value < 0.05 (based on Friedman χ^2 statistic)
Nemenyi Post Hoc test	Identifies which pairs of models differ significantly	Critical Difference (CD) formula
Critical Difference Diagram	Visualizes model rank differences and significance relationships	Uses CD from the Nemenyi test

3. Results and Discussion

Analysing climatic variability, detecting trends, and assessing regional distribution is essential for gaining deep insights into the implications of climate change and enhancing resource and infrastructure planning. Meteorological data is an essential source of knowledge for comprehending these alterations. Detecting trends in time series data without assuming component distributions is a major benefit of non-parametric tests in climate research. Weather factors, such as temperature, wind speed, precipitation, and humidity, can be measured in various sizes with these tests. Examining spatial distribution is essential to understanding local alterations in climatic variables and their historical changes (Ampofo et al., 2023).

3.1. Temporal trend analysis

3.1.1. Heatwave trends in the USA

Due to global warming, the temperature on Earth is increasing rapidly now. For mitigation of this trait, we need to know the pattern of the increase in heat. This study focuses on the pattern following which temperature is increasing. This might help take the necessary actions globally and regionally to minimize the aftermath of the heatwaves that are affecting human lives, agriculture, economy and every other aspect of lives. An annual spatial and temporal trend of heatwave frequencies in USA across 20 years (2000-2019) is depicted in **Fig 3.1.**

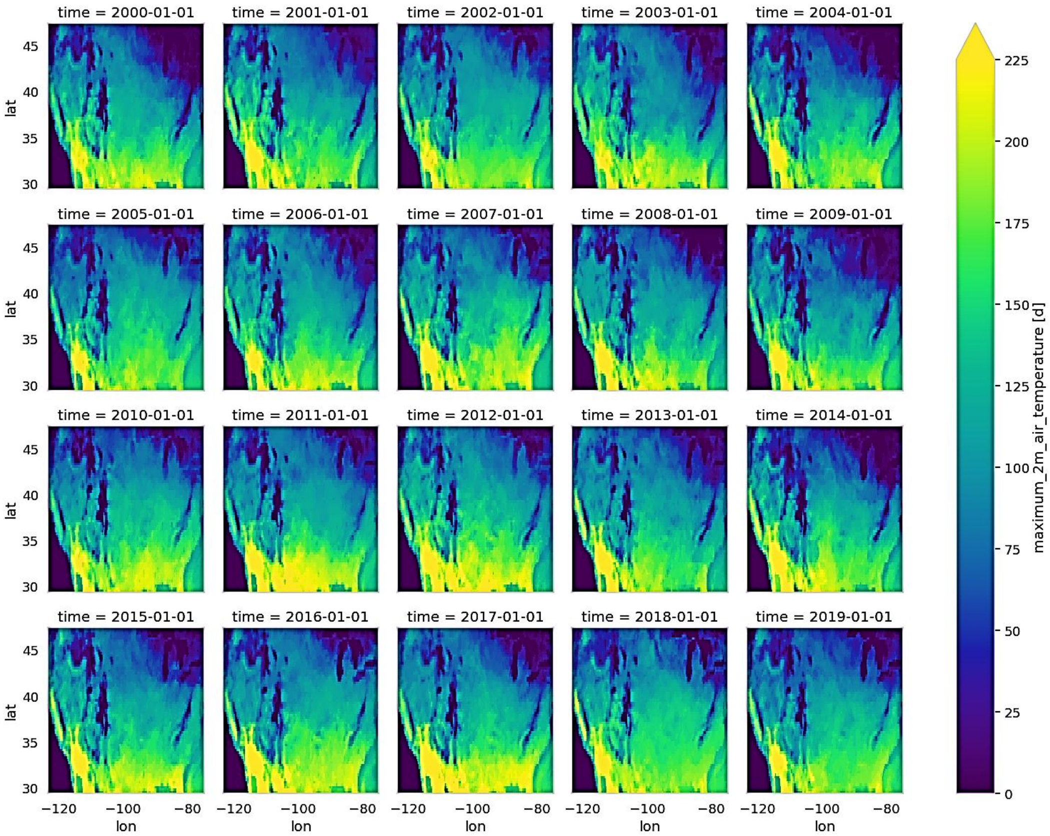

Fig. 3.1: Annual Trend of Heatwave Frequency or Spatial and temporal evolution of heatwave frequency over 20 years across the continental U.S

This figure highlights a warming trend with significant public health, environmental, and socio-economic impacts. It provides a clear visual confirmation of increasing extreme heat events under a changing climate. Each subplot depicts one year (from 2000 to 2019), labeled by its starting date (e.g., time = 2000-01-01). The latitudinal and longitudinal coverage covers the contiguous United States (roughly 30°N to 50°N and -125°W to -70°W). The color scale shows the number of heatwave days per year at each location, with warmer colors (yellow) indicating more days.

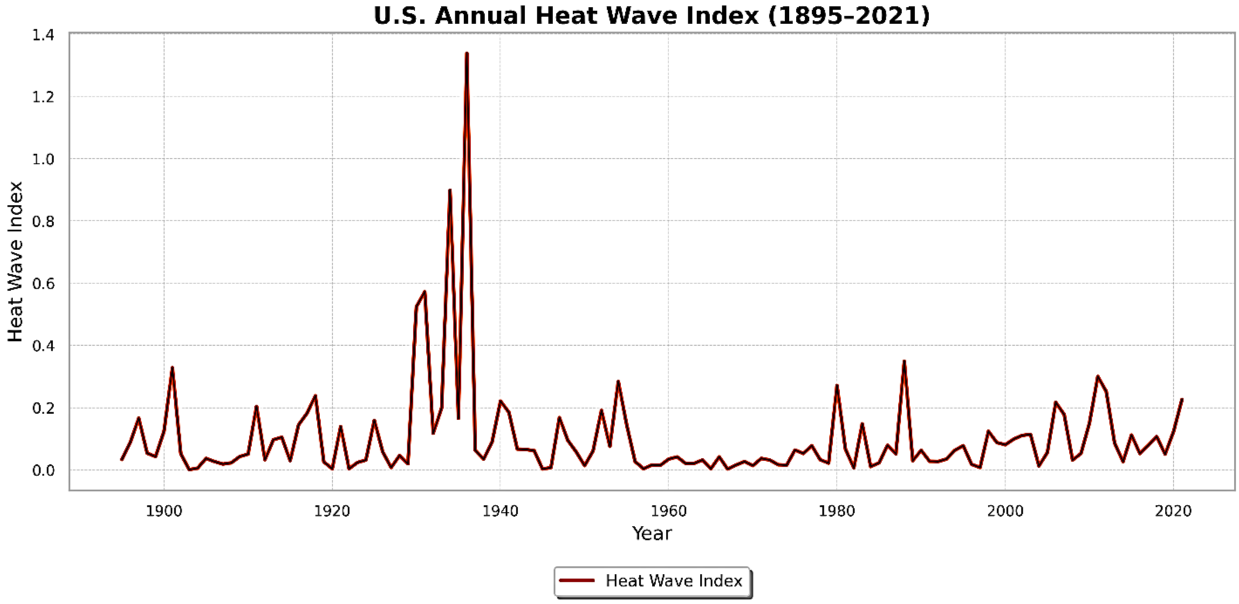

Fig. 3.2: Annual heatwave index (HWI) of the USA across 1895-2021

The graph in **Fig. 3.2** illustrates the trend of the U.S. annual Heat Wave Index (HWI) from 1895 to 2021, showing how frequently and how severe heatwave events have been nationwide. The HWI is a unitless measure that tracks the persistence of unusually high temperatures over consecutive days. A notable spike appears in the 1930s during the Dust Bowl era, characterized by prolonged droughts and record heat waves (Carrasco et al.,2024).. After this period, the index remains relatively stable with occasional fluctuations until a gradual increase becomes evident in recent decades, especially since the late 1990s. This upward trend aligns with broader evidence of human-induced climate change and suggests an increase in extreme heat events over time. The graph emphasizes the growing importance of monitoring heatwaves for climate risk assessment and public health planning.

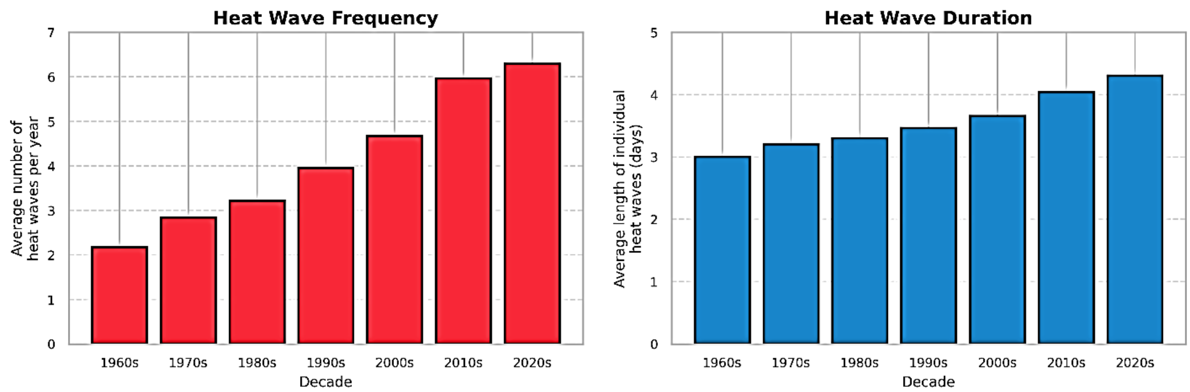

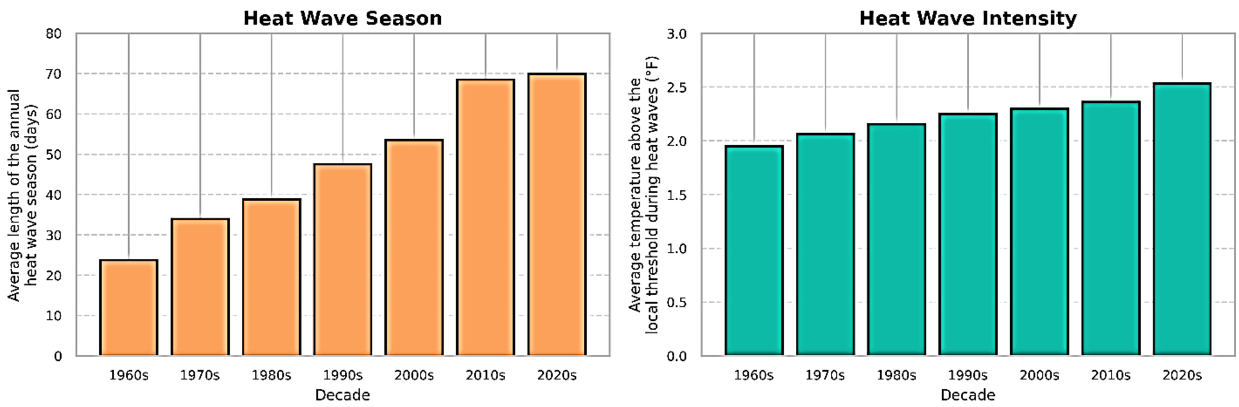

Fig. 3.3: Average decadal heat wave frequency, duration, season, and intensity in the USA

Fig. 3.3 illustrates a gradual increase in all heatwave characteristics. The frequency of heatwaves has been rising each decade, indicating that this trend will likely continue in the future. While the duration of heatwaves steadily increased until the 1990s, it experienced a sharper rise in subsequent decades. The length of the heatwave season has also been extending, from 20 days in the 1960s to 70 days now, an alarming development. Meanwhile, the intensity of heatwaves remains relatively stable but is still increasing alongside temperature rises. Even slight fluctuations in temperature can lead to significant impacts on Earth and its ecosystems. Overall, all heatwave parameters show an upward trend, suggesting that they will continue to escalate in the coming decades.

3.1.2. Historical Heatwave Trends in the Key Counties

Over the past two decades, the region has experienced a notable shift in heatwave patterns, marked by a color progression from green to yellow, particularly across central and eastern Kansas and Arkansas, indicating a steady rise in the number of annual heatwave days in **Fig. 3.4.** While Nebraska and Iowa, located further north, showed more modest increases, there has been a clear upward trend in heatwave frequency since 2010. Southern Kansas and nearly all of Arkansas have consistently surpassed 100 heatwave days per year during the 2010s. Notably, areas in Nebraska and Iowa that experienced fewer than 25 heatwave days annually in the early 2000s are now facing between 50 and 100+ days by 2019, signaling a northward expansion of extreme heat conditions.

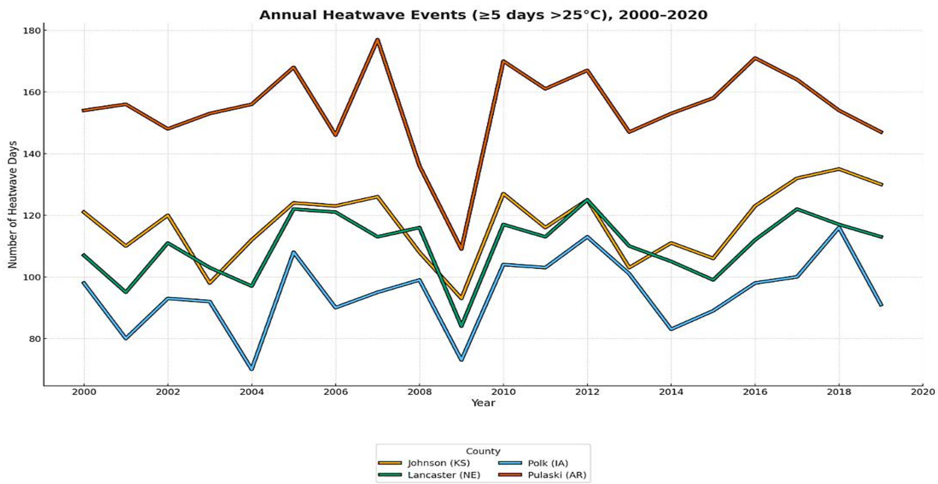

Fig. 3.4: Annual Heatwave events in key counties

3.1.3. Climatological Shifts and Emerging Heatwave Dynamics in the KANI Region

Increasingly dry summers, especially in Kansas and Nebraska, have reduced evaporative cooling, leading to faster surface warming. Agricultural intensification has altered land surface properties like albedo and roughness, subtly shifting the local energy balance. At the same time, persistent high-pressure systems, “heat domes”, have become more common, limiting air circulation and intensifying heat. These changes pose serious risks: outdoor workers and the elderly face greater heat-related health threats, while crops like corn and soybeans are vulnerable to high temperatures during flowering, impacting yields. Rising irrigation demands and declining aquifer recharge, particularly in the Ogallala Aquifer, further strain water resources. Observed data show a clear rise in heatwave frequency across the KANI region (Kansas, Nebraska, Iowa), along with a northward shift of extreme heat events, signs that this area is becoming a climate-sensitive hotspot. These trends closely mirror global climate model projections, emphasizing the urgent need for localized adaptation strategies.

3.1.4 Temperature trend (2000-2024) in Key counties

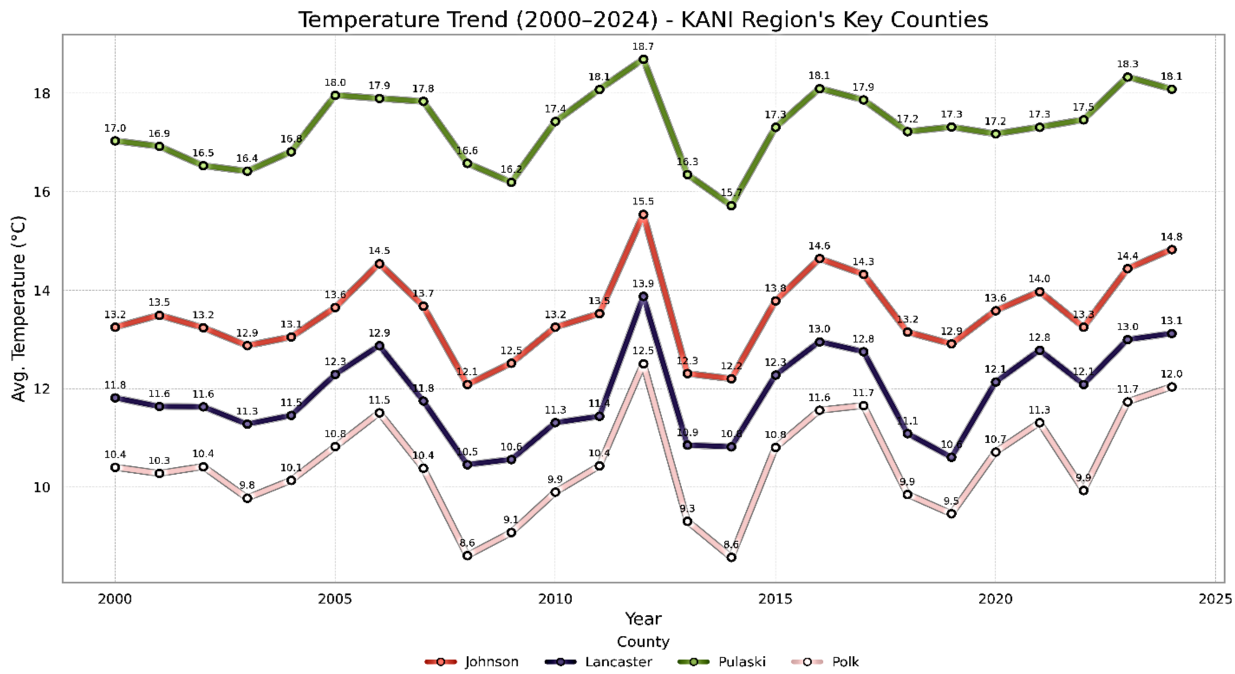

Fig. 3.5: Average temperature trends from 2000-2024 in key counties

Fig. 3.5 illustrates the interannual variation in average air temperature across four representative counties-Johnson, Lancaster, Pulaski, and Polk, from 2000 to 2024. While year-to-year fluctuations are apparent in all counties, Pulaski consistently exhibits higher mean temperatures compared to the others, with values largely ranging between 17°C and 18.7°C. In contrast, Polk records the lowest annual averages throughout the period, often remaining below 12°C. A general warming tendency is visible in all four counties, with the recent decade showing elevated temperature levels relative to the early 2000s. Despite minor cooling anomalies in years such as 2010 and 2014, the long-term trend supports the broader narrative of regional warming. This pattern aligns with global temperature rise and the USA national trends and highlights the growing relevance of localized heat monitoring for climate adaptation planning.

3.1.5. Seasonal Temperature Trend in Key Counties

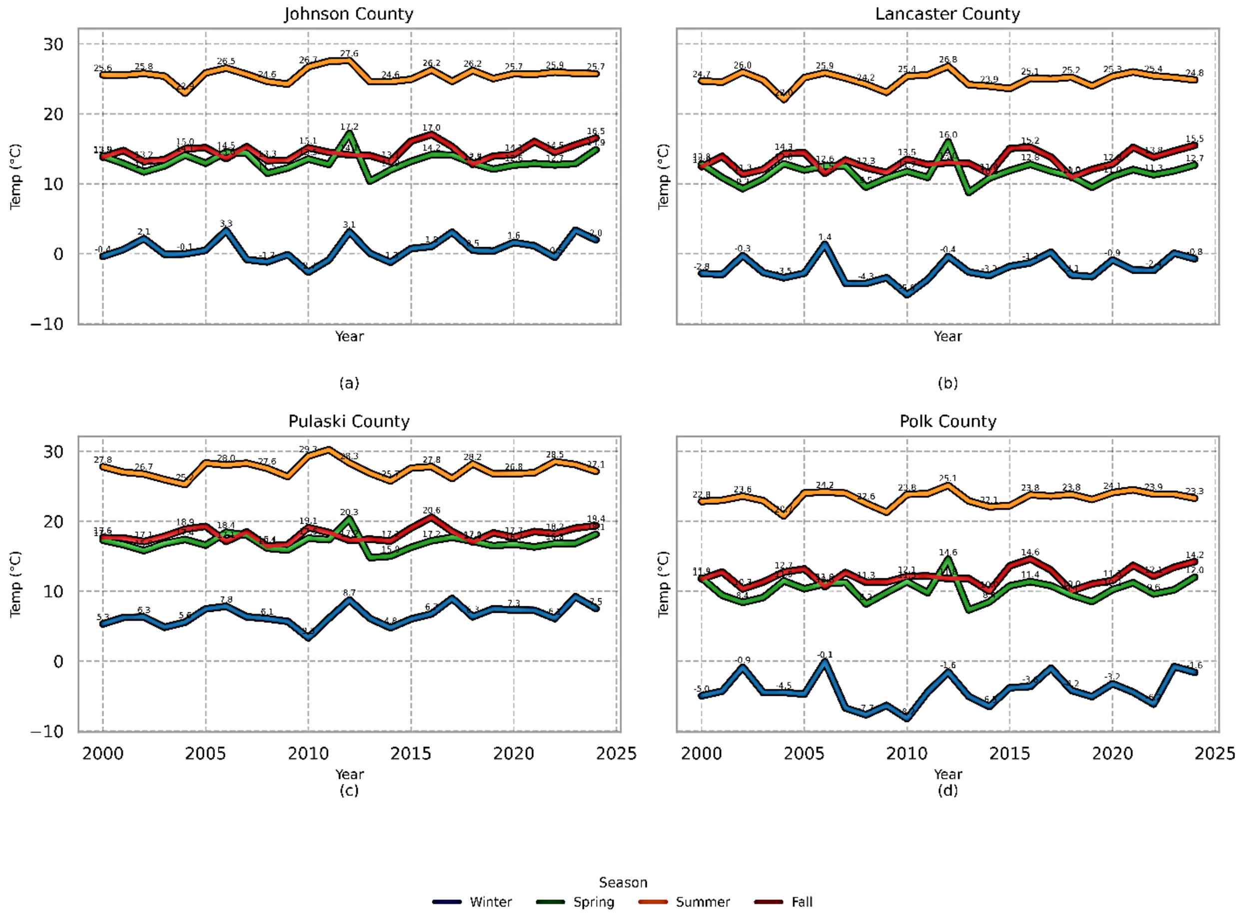

Fig. 3.6: Seasonal temperature characteristics of key counties

Fig. 3.6 (a)-(d) track winter, spring, summer, and autumn mean temperatures for Johnson, Lancaster, Pulaski, and Polk Counties, respectively. In every county, summer (orange) remains the warmest season, averaging 24–29 °C, while winter (navy) registers the lowest values, frequently dipping below 0 °C in Polk. Pulaski exhibits the consistently highest seasonal means across the record, whereas Polk remains the coolest. Despite year-to-year variability, most evident in the 2010 cold anomaly and the 2012 warm spring pulse, all four counties show a subtle upward drift in seasonal means, with the most pronounced relative increases occurring in winter and spring. This season-specific warming pattern aligns with broader mid-latitude climate trends and underscores the heightened risk of early-season heat stress and reduced winter chill in the region.

3.1.6. Monthly Temperature Trend in Key Counties

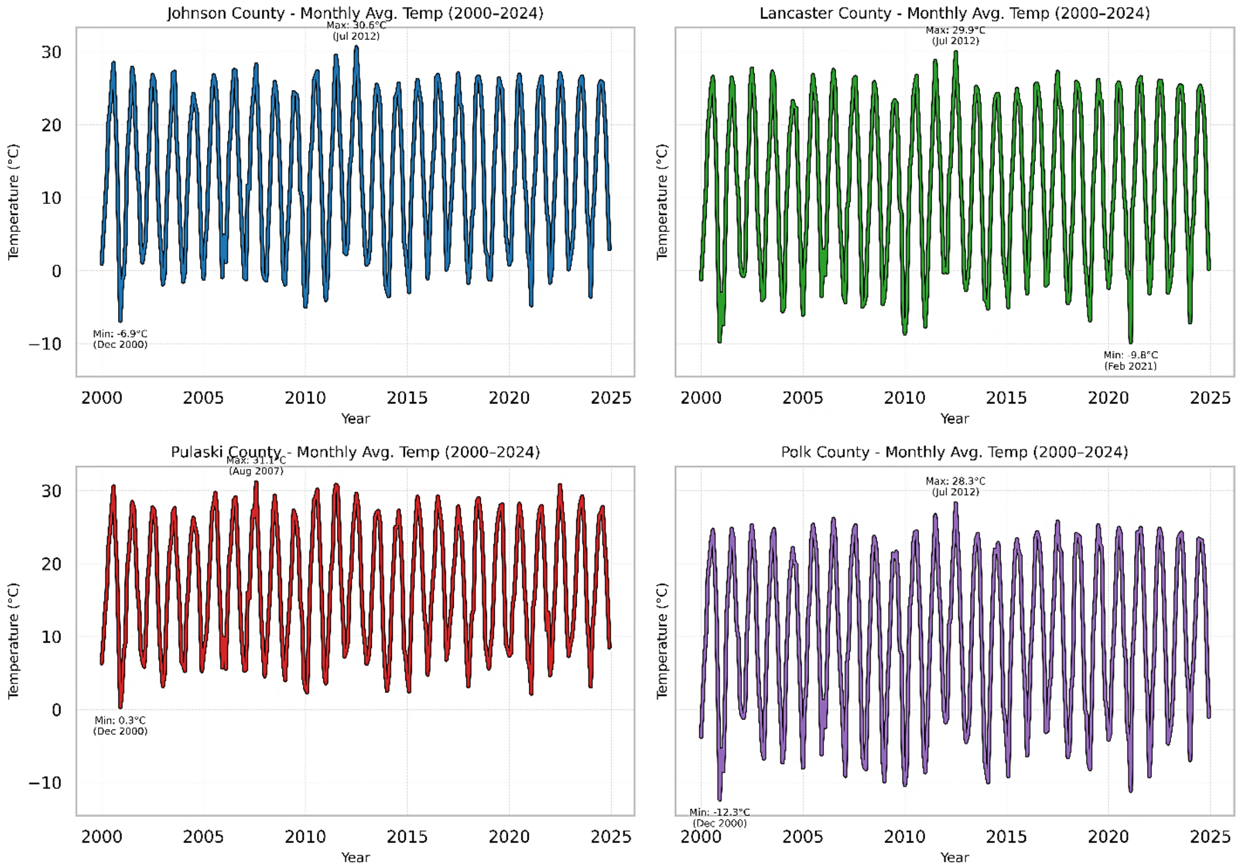

Fig. 3.7: Seasonal temperature characteristics of key counties

The four plots in **Fig. 3.7** illustrate long-term monthly mean air temperature variations for Johnson, Lancaster, Pulaski, and Polk Counties from 2000 to 2024. All counties exhibit a distinct seasonal cycle, characterized by sinusoidal temperature oscillations driven by annual solar forcing. Summer peaks typically range between 25 °C and 32 °C, while winter minima span from -12.3 °C (Polk, Dec 2000) to approximately -6.9 °C (Johnson, Dec 2000). The July 2012 extreme heat event is evident in all counties, marking the historical maximum in Johnson (31 °C), Lancaster (29.7 °C), and Polk (28.3 °C), whereas Pulaski's warmest month occurred in August 2007 (31.9 °C). Pulaski consistently exhibits higher average temperatures, while Polk maintains the lowest seasonal means across the observation period. A gradual post-2010 rise in both winter lows and summer means is observable, aligning with broader regional warming patterns. These monthly trends provide high-resolution evidence of shifting climate baselines, underscoring the importance of seasonal dynamics in long-term temperature escalation.

3.2. Temperature Trend Prediction (2000-2024) of key counties

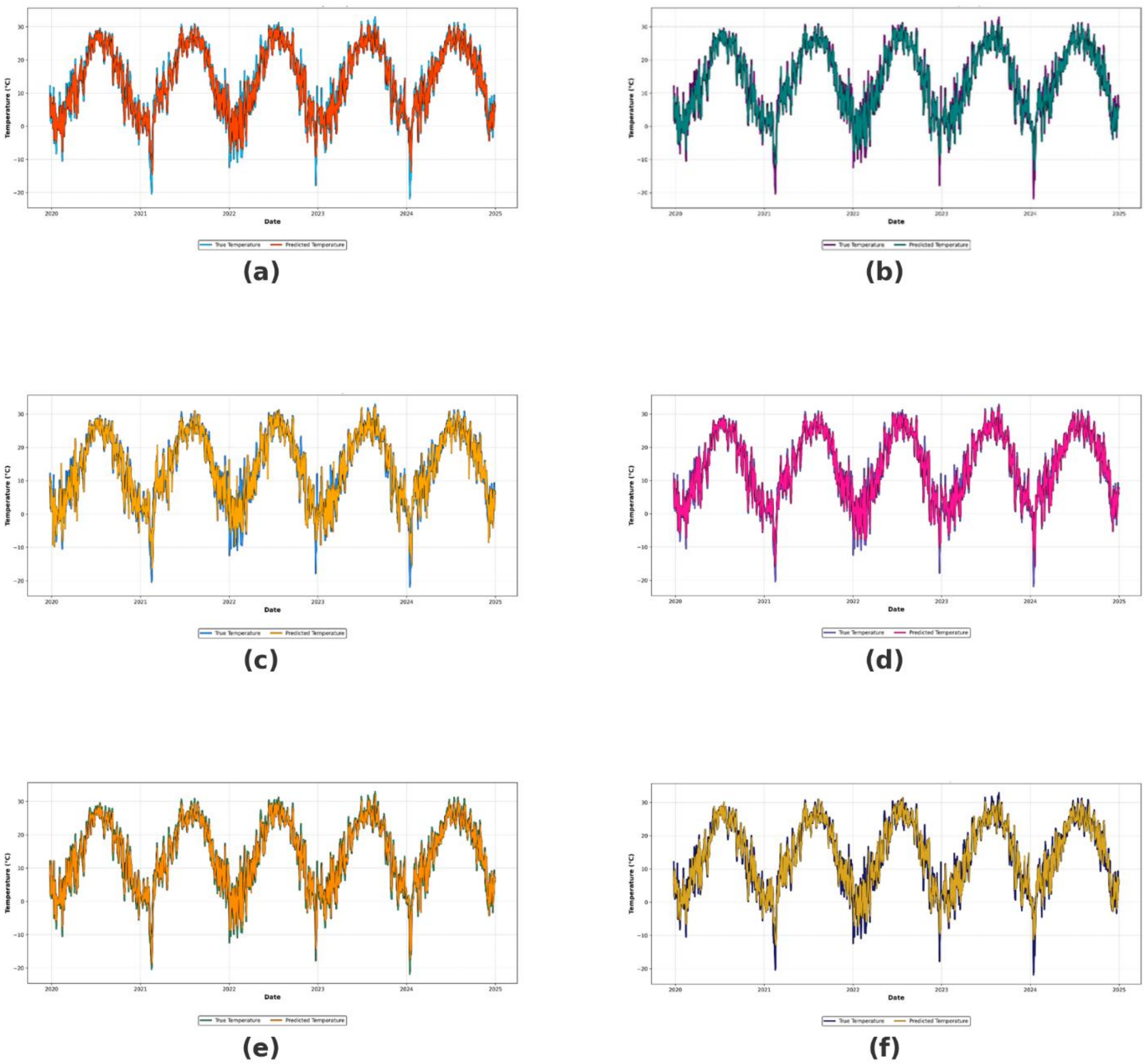

Fig. 3.8: Daily Temperature Prediction using (a) XGBoost Regression Model, (b) Random Forest Model, (c) Decision Tree Model, (d) SVR Model, (e) Linear Regression Model, (f) KNN Model (2020–2024) for Johnson County, Kansas, USA

The **Fig. 3.8** illustrates daily temperature predictions from six machine learning models compared to observed values in Johnson County over the period 2020–2024. All models effectively capture the dominant seasonal cycle, reflecting annual temperature variations ranging from approximately –15 °C in winter to over 30 °C in summer. Ensemble methods, particularly RF and XGBoost, demonstrate the highest consistency, maintaining prediction errors within ±2 °C for the majority of days while closely preserving both peak intensity and seasonal timing. KNN also follows the observed trend well, though it tends to underestimate summer highs by 1-2 °C. SVR introduces larger deviations during winter, with cold extremes occasionally overpredicted by more than 5 °C, indicating sensitivity to abrupt thermal drops. The DT model captures seasonal timing but exhibits a segmented appearance due to its sensitivity to daily noise, suggesting limited generalization capacity. LR performs the weakest overall, underestimating both summer and winter extremes by up to 4 °C and flattening transitional periods. Notably, all models show increased residuals during rapid temperature shifts, particularly in early 2021 and mid-2023, highlighting a common limitation in capturing short-term fluctuations. Overall, ensemble-based models provide more reliable and temporally stable performance for daily temperature forecasting in this region.

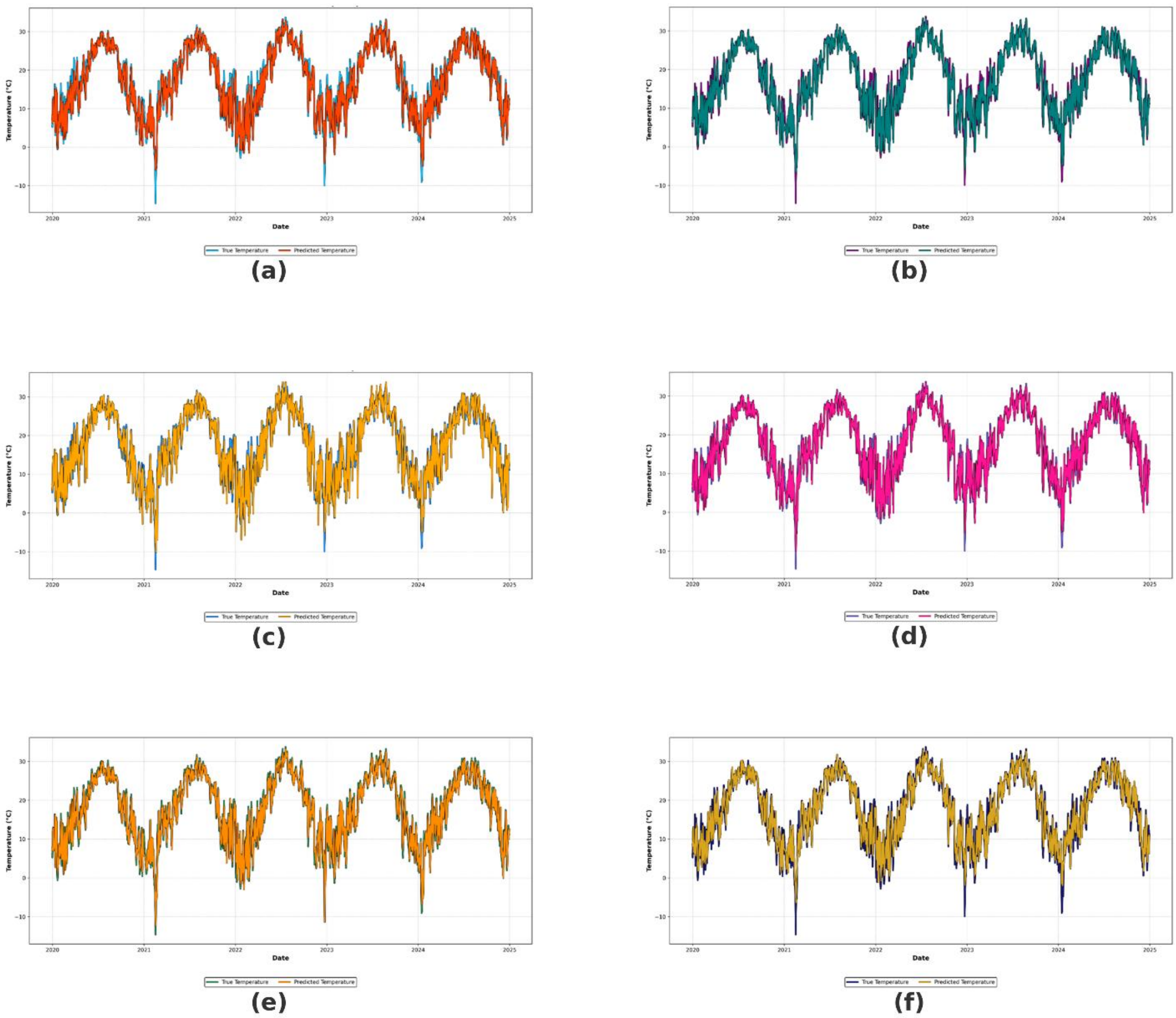

Fig 3.9: Daily Temperature Prediction using (a) XGBoost Regression Model, (b) Random Forest Model, (c) Decision Tree Model, (d) SVR Model, (e) Linear Regression Model, (f) KNN Model (2020–2024) for Pulaski County, Arkansas, USA

The **Fig. 3.9** presents temperature prediction results for Pulaski County (2020–2024) using six machine learning models, evaluated against observed daily temperatures. Across all panels, the models successfully replicate the region's distinct annual thermal cycles, marked by summer peaks exceeding 30 °C and winter lows dipping below 0 °C. Ensemble-based models, particularly Random Forest and XGBoost (panels e and f), demonstrate strong alignment with true values, preserving both the shape and amplitude of seasonal transitions with error margins largely confined within ±2 °C. KNN (panel c) tracks the overall trend but exhibits slight underestimation during heatwave periods, with predicted highs trailing actual values by up to 2.5 °C. Support Vector Regression (panel b) maintains structural consistency but shows moderate overshooting in colder months, particularly during sharp winter declines. The Decision Tree model (panel d) captures the seasonal timing but introduces abrupt jumps in transitional periods, reflecting its tendency toward overfitting local noise. Linear Regression (panel a) underestimates extremes at both ends of the temperature spectrum and flattens the curve during rapid seasonal shifts, suggesting limited capability in modelling nonlinearity. Notably, performance drops are observed across models during periods of sharp temperature fluctuation, especially around early 2021 and mid-2023, highlighting the models' shared difficulty in capturing short-term thermal variability. Overall, ensemble models stand out in this county as well for their robust seasonal sensitivity and minimized deviation, making them preferable for daily temperature forecasting in Pulaski County.

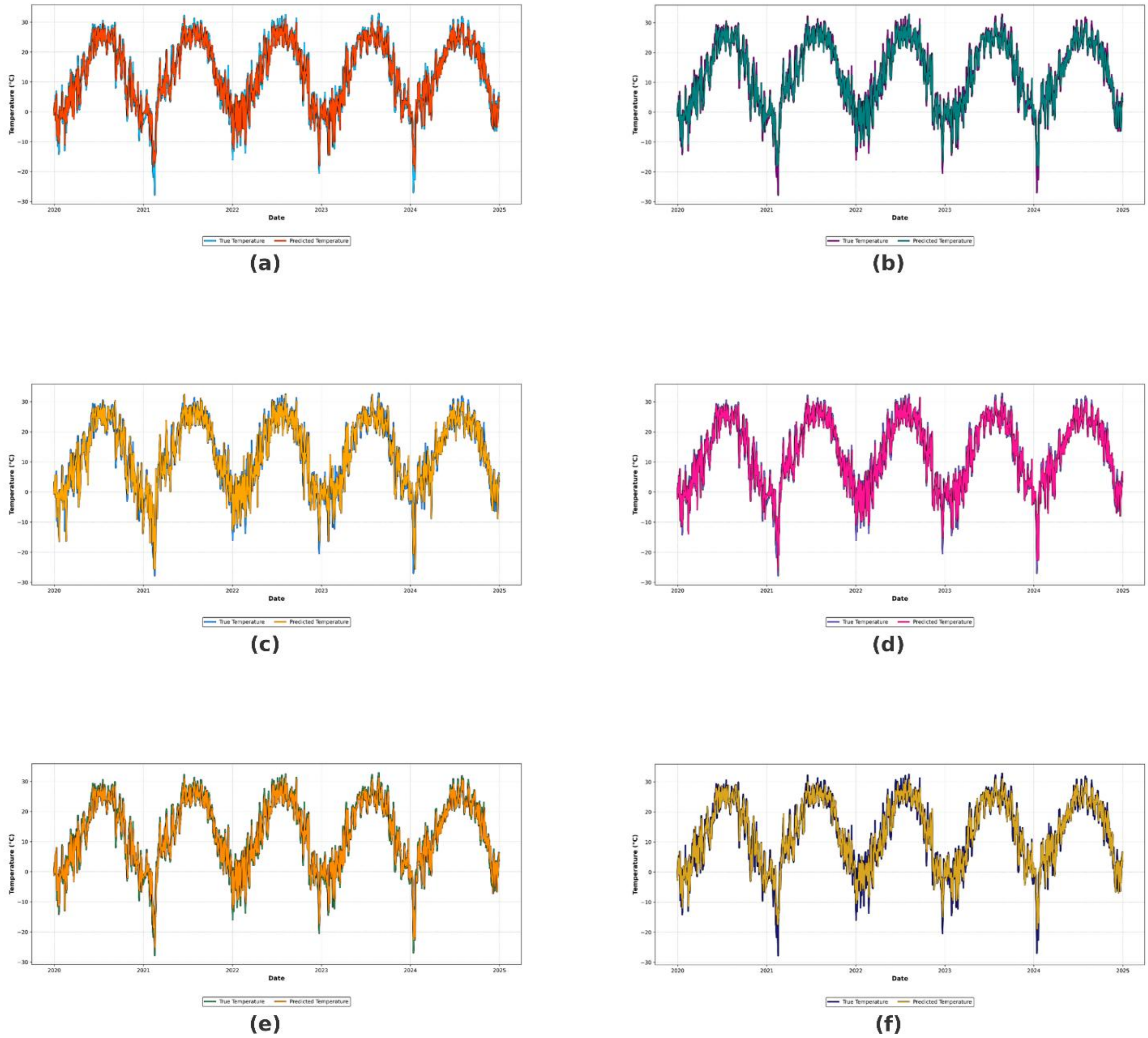

Fig. 3.10: Daily Temperature Prediction using (a) XGBoost Regression Model, (b) Random Forest Model, (c) Decision Tree Model, (d) SVR Model, (e) Linear Regression Model, (f) KNN Model (2020–2024) for Lancaster County, Nebraska, USA

Fig. 3.10 presents the daily temperature predictions for Lancaster County from 2020 to 2024, generated by six machine learning models. All models successfully captured the cyclical seasonality of temperature, with summer peaks consistently reaching between 26°C and 31°C, and winter lows dropping as far as –11.2°C. The highest predicted temperature occurred in mid-2022, reaching 30.7°C, while the coldest dip was recorded in early 2023 at –11.2°C. Year-to-year patterns showed minor fluctuations, with the seasonal amplitude remaining relatively stable throughout the observed period. Models such as RF and XGBoost produced smoother and more consistent transitions between seasons, while SVR and KNN showed slightly more noise during seasonal changes, especially in spring and fall. Compared to the other counties, Lancaster County's temperature trends showed relatively milder winter extremes and a narrower range of interannual variation, potentially indicating stronger urban heat retention effects. These preliminary results offer a reliable depiction of temperature dynamics and will serve as the basis for further validation and accuracy assessment.

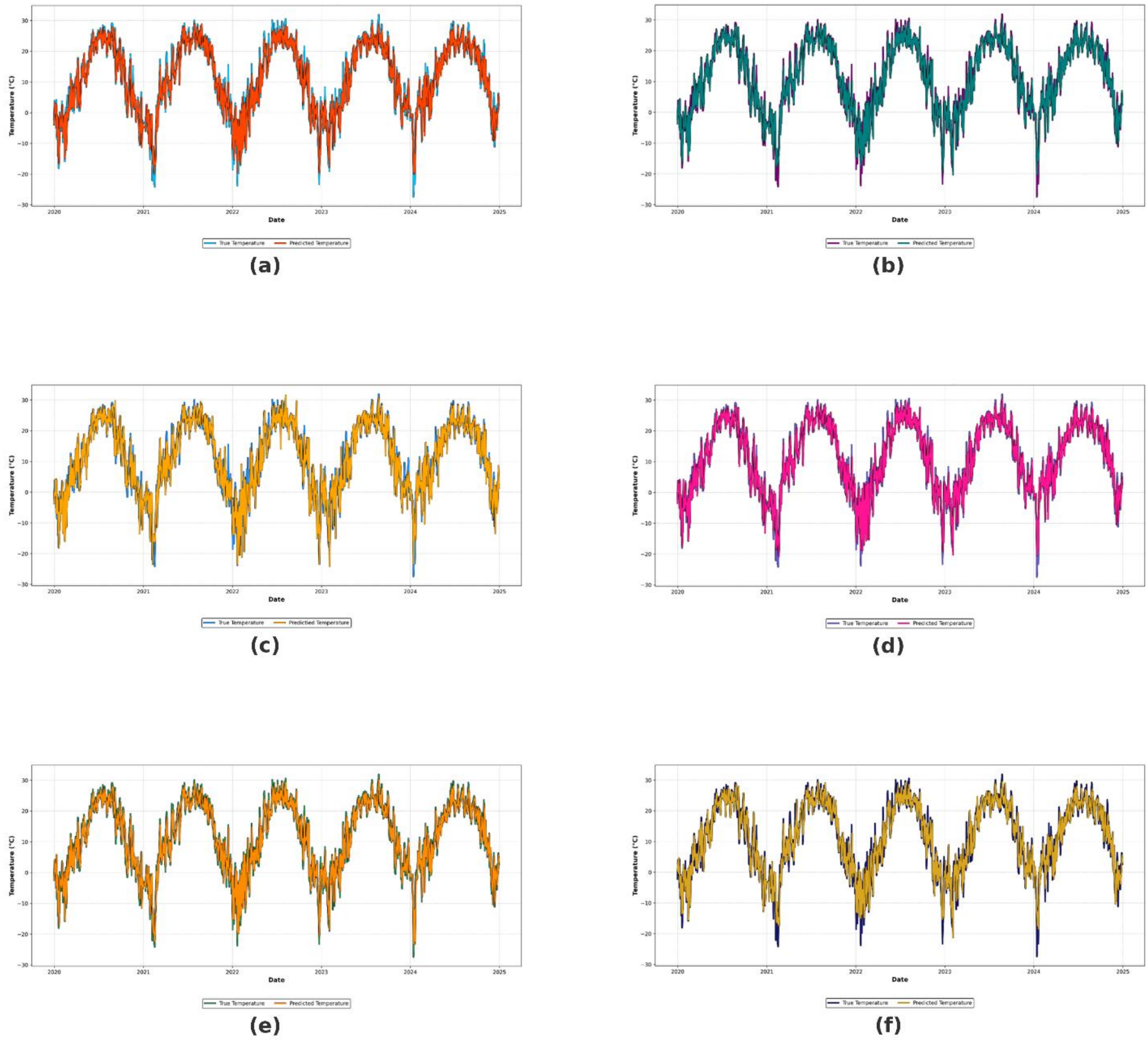

Fig. 3.11: Daily Temperature Prediction using (a) XGBoost Regression Model, (b) Random Forest Model, (c) Decision Tree Model, (d) SVR Model, (e) Linear Regression Model, (f) KNN Model (2020–2024) for Polk County, IA

Fig. 3.11 compares observed daily temperatures in Polk County with predictions from six machine-learning models over 2020–2024. The models reproduce the seasonal cycle typical of this cooler Midwestern County, with summer highs of 26–29 °C and winter lows of –10 °C to –12 °C. RF and XGBoost maintain the closest visual agreement with the observations, preserving both amplitude and timing of seasonal transitions. KNN follows the overall pattern but shows a warm bias of approximately 1 °C during late-summer peaks. SVR traces mid-range temperatures accurately yet overshoots sharp winter declines, most noticeably during the February 2021 cold spell. The DT track mirrors seasonal timing but introduces abrupt stepwise fluctuations, indicating sensitivity to daily noise, whereas LR underestimates both extremes and smooths transitional periods. Compared to the warmer counties in the study, Polk experiences smaller yearly temperature swings and fewer sharp spikes, highlighting the effects of local climate moderation. These prediction curves offer an initial look at how the models perform; a detailed quantitative evaluation will be presented in the next section.

3.3. Model Accuracy Assessment

3.3.1. Model Evaluation Metrics

To assess the level of accuracy of the temperature prediction models, a combination of standard performance metrics and statistical validation techniques was employed. Specifically, the coefficient of determination (R^2), root mean square error (RMSE), and mean absolute error (MAE) were calculated to evaluate how well the models performed in observing temperature patterns from 2020-2024. These metrics provided insight into both quantitative and qualitative measures and direction of prediction errors, allowing for direct comparison of model accuracy. To further examine whether differences in model performance were statistically significant, a Friedman test was conducted across all models for all the counties. This non-parametric test evaluated the relative ranking of models without assuming normality of error distributions. Upon finding significant differences, a Nemenyi post-hoc test was applied to determine which pairs of models differed meaningfully in performance. The results were visualized using a Critical Difference (CD) diagram, which clearly illustrated the comparative effectiveness of each model based on its average rank. This two-stage validation, blending quantitative accuracy with robust statistical inference, ensured a comprehensive and fair assessment of model reliability across varying climatic conditions in the KANI region. All the values of R^2, RMSE, and MAE of all six models are listed in **Table.7**-

Table. 7: Comparison of Accuracy Metrics for ML Models Applied to Urban Temperature Trends

Metric Score (County-wise)					
Model	**Evaluation Metrics**	**Johnson**	**Lancaster**	**Pulaski**	**Polk**
KNN	R^2	0.8854	0.8930	0.8850	0.8904
	RMSE	3.51	3.74	2.95	3.84 °C
	MAE	2.60	2.83	2.15	2.83 °C
Linear Regression	R^2	0.8118	0.8145	0.8132	0.8127
	RMSE	3.88	3.84	3.56	3.83°C

	MAE	3.27	3.49	3.85	3.51°C
Decision Tree	R^2	0.8742	0.8807	0.8669	0.8721
	RMSE	3.68	3.94	3.18	4.15°C
	MAE	2.66	2.84	2.22	2.96°C
SVR	R^2	0.9098	0.9122	0.9085	0.9067
	RMSE	3.12	3.38	2.63	3.54°C
	MAE	2.25	2.48	1.83	2.52°C
RF	R^2	0.9063	0.9095	0.9064	0.9083
	RMSE	3.18	3.43	2.66	3.51°C
	MAE	2.33	2.54	1.91	2.57°C
XGBoost	R^2	0.91	0.91	0.91	0.91
	RMSE	3.18	3.40	2.60	3.52°C
	MAE	2.34	2.50	1.88	2.55°C

Table 4 details the model performance across Johnson, Lancaster, Pulaski, and Polk counties from 2020 to 2024. XGBoost achieved the strongest and most consistent performance, with R^2 values of 0.91 in all counties, RMSE ranging from 2.60 °C (Pulaski) to 3.52 °C (Polk), and MAE between 1.88 °C and 2.55 °C. SVR closely followed with R^2 scores between 0.9085 and 0.9122, though RMSE values (2.63–3.54 °C) were slightly higher than XGBoost, particularly in colder regions like Polk. Random Forest also performed reliably, maintaining R^2 above 0.906 and MAE below 2.57 °C in all counties.

In contrast, Decision Tree and KNN models demonstrated larger error margins. For instance, DT's RMSE reached 4.15 °C in Polk, and KNN's RMSE rose to 3.84 °C, indicating sensitivity to noise and reduced generalizability. Linear Regression, while computationally efficient, underperformed overall, with R^2 values around 0.81 and MAE peaking at 3.51 °C in Polk. These results closely reflect the visual assessments from Figures 3.8–3.11, where XGBoost and RF best followed seasonal extremes, and simpler models visibly lagged during rapid temperature transitions.

3.3.2. Friedman and Nemenyi Post Hoc Test

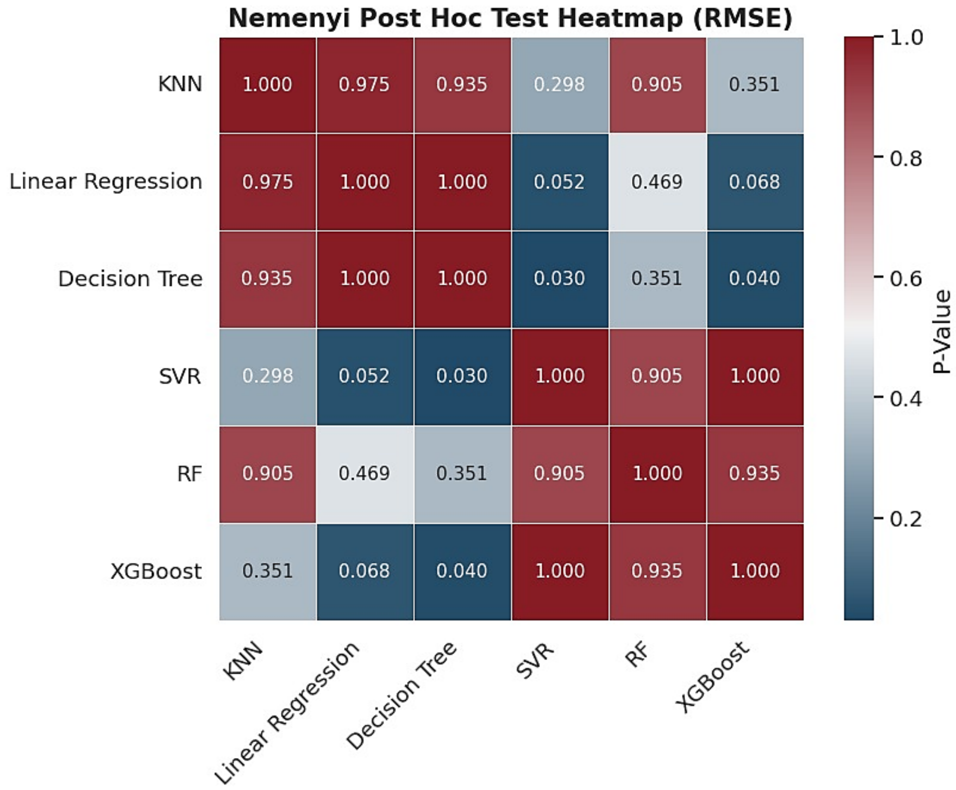

Fig. 3.12: Nemenyi Post Hoc test heatmap

Fig. 3.12 presents the pairwise p-value matrix derived from the Nemenyi post-hoc test following Friedman's ranking analysis of six regression models evaluated across four counties, using RMSE as the primary performance metric. Each matrix cell indicates the probability that two models are statistically equivalent in terms of their average rank; values below 0.05 (shaded in cooler tones) denote a statistically significant difference at the 95% confidence level. The test identifies two statistically significant contrasts: Decision Tree vs. SVR ($p = 0.030$) and Decision Tree vs. XGBoost ($p = 0.040$). These results confirm that the Decision Tree model underperforms compared to SVR and XGBoost with statistical certainty. Other model comparisons, including those between KNN, Linear Regression, Random Forest, and the top performers, all yield p-values above the 0.05 threshold, indicating no significant differences in their rankings. For example, KNN vs. SVR ($p = 0.298$), RF vs. XGBoost ($p = 0.935$), and Linear Regression vs. SVR ($p = 0.052$) suggest performance similarities from a statistical standpoint. Overall, the test reinforces that while small numerical differences in RMSE exist across models, only Decision Tree is conclusively less effective than the top-ranked methods. Ensemble-based regressors (Random Forest and XGBoost) along with SVR and KNN form a performance cluster with statistically indistinguishable accuracy across counties, supporting their recommendation for robust, regionally transferable temperature forecasting.

3.3.3. Visualization of Critical Differences between Models

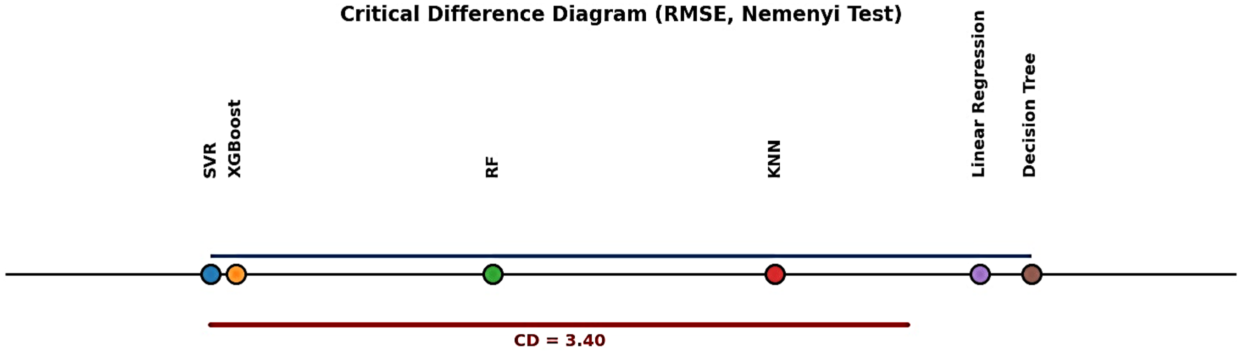

Fig. 3.13: Critical difference diagram of models

Fig. 3.13 shows the average Friedman ranks of six regressors, calculated from their RMSE scores across four Midwestern counties. The horizontal axis (labeled Average Friedman rank; lower = better) indicates that XGBoost (rank = 2.00), SVR (2.25), Random Forest (2.75), and KNN (3.00) are grouped within a single blue bar whose span (≤ 3.40 rank units) is shorter than the critical-difference value CD = 3.40. Therefore, the Nemenyi post-hoc test cannot distinguish these four algorithms at the 95% confidence level; they form a statistically equivalent, high-performance cluster. To the right, Linear Regression (rank = 5.00) and Decision Tree (rank = 5.75) fall outside the blue segment. Their rank gaps relative to XGBoost (Δ = 3.00 and 3.75, respectively) exceed the CD threshold, indicating that both models are significantly less accurate than any member of the top cluster. The distance between Linear Regression and Decision Tree (Δ = 0.75) is below CD, so no significant difference exists within this lower-performing pair. Overall, for daily temperature forecasting over the study area, any of the four top-ranked models, especially the ensemble tree methods (XGBoost, Random Forest), are suitable choices; SVR and KNN offer similar accuracy with different computational trade-offs. Linear Regression and Decision Tree should only be used if simplicity is more important than forecast accuracy.

4. Conclusion

I. Nationwide escalation of heatwaves (2000-2019): Annual maps show a clear warming trend across the CONUS, with more than 100 heat-wave days per year, becoming frequent in southern Kansas and Arkansas after 2010.

II. Decadal metrics confirm upward momentum: Heat-wave frequency, duration, seasonal length, and intensity all rise each decade; the heat-wave season has stretched from almost 20 days (1960s) to close to 70 days after 2020s.

III. KANI region as an emerging hotspot: Johnson (KS), Pulaski (AR), Lancaster (NE) and Polk (IA) now exhibit more frequent and earlier-season heat extremes, driven by drier summers, land-use change, and persistent summer blocking highs.

IV. County-scale warming (2000-2024): Pulaski is the warmest (17–18.7 °C), Polk exhibits the coolest (< 12 °C); all counties' temperatures rose faster after 2010, especially in winter and spring.

V. Daily prediction skill of ML models: Ensemble trees (XGBoost, Random Forest) track seasonal cycles within ±2 °C; SVR slightly overshoots winter extremes; KNN underestimates summer peaks; Decision Tree is noisy, and Linear Regression dampens extremes.

VI. Quantitative accuracy: XGBoost yields the lowest MAE (1.88–2.55 °C) and RMSE (2.60–3.52 °C) with $R^2 = 0.91$, closely followed by SVR and Random Forest; Linear Regression lags ($R^2 = 0.81$, MAE up to 3.51 °C), Decision Tree shows the largest RMSE (4.15 °C in Polk).

VII. Statistical inference: The Nemenyi test identified statistically significant performance gaps between Decision Tree and both SVR and XGBoost ($p < 0.05$), confirming its relative underperformance. The critical difference diagram further illustrates this by showing Decision Tree and Linear Regression outside the top-performing cluster formed by SVR, XGBoost, Random Forest, and KNN. Although Linear Regression did not differ significantly in pairwise comparisons (e.g., $p = 0.052$ vs SVR), its rank exceeded the critical threshold, indicating a slight but consistent decline. Overall, these results support the reliability of ensemble and kernel-based models for accurate regional temperature forecasting.

VIII. Operational recommendation: For county-scale temperature forecasting, ensemble trees (XGBoost and RF) are recommended, whereas SVR and KNN are acceptable alternates, and Linear Regression and Decision Tree should be reserved for low-complexity use-cases.

Acknowledgements

The authors extend their sincere appreciation to the organizations and platforms that made high-quality environmental data openly accessible, including the European Centre for Medium-Range Weather Forecasts (ECMWF) for the ERA5-Land dataset and the teams behind Google Earth Engine for providing essential cloud-based computing resources. Additional thanks are due to the U.S. Census Bureau and NOAA for their continued commitment to maintaining public datasets that are crucial for climate research.

Data Availability Statement

All relevant data will be made available upon request to corresponding author.

Conflict of Interest

The authors declare no conflict of interest.

References

Abu-Shaira, M., & Shi, W. (2024, August). Unveiling Statistical Significance of Online Regression Over Multiple Datasets. In *2024 IEEE 7th International Conference on Multimedia Information Processing and Retrieval (MIPR)* (pp. 274-279). IEEE.

Ali, M., Mukarram, M. M. T., Chowdhury, M. A., Karin, S., & Faruq, A. N. (2021). Integration & implication of machine learning: barriers to aid environmental monitoring & management. *Open Access Library Journal, 8*(6), 1–13.

Brimicombe, C., Runkle, J. D., Tuholske, C., Domeisen, D. I., Gao, C., Toftum, J., & Otto, I. M. (2024).

Preventing heat-related deaths: The urgent need for a global early warning system for heat. *PLOS Climate, 3*(7), e0000437.

Carrasco Galvan, G. B., Vadjunec, J. M., & Fagin, T. D. (2024). Lessons from the Archives: Understanding Historical Agricultural Change in the Southern Great Plains. *Land*, *13*(2), 196.

Camps-Valls, G., Fernández-Torres, M. Á., Cohrs, K. H., Höhl, A., Castelletti, A., Pacal, A., ... & Williams, T. (2025). Artificial intelligence for modeling and understanding extreme weather and climate events. *Nature Communications, 16*(1), 1919.

Copernicus Climate Change Service (C3S) (2017): ERA5: Fifth generation of ECMWF atmospheric reanalyses of the global climate. Copernicus Climate Change Service Climate Data Store (CDS), (5 June,2025), https://cds.climate.copernicus.eu/cdsapp#!/home

Das, A., Shuvo, R. M., Mukarram, M. M. T., & Sharno, M. A. (2024). Navigating the energy policy landscape of Bangladesh: A stern review and meta-analysis. *Energy Strategy Reviews, 52*, 101336.

Dawar, I., Negi, S., & Chauhan, A. (2024). Explainable AI for Next Generation Agriculture—Current Scenario and Future Prospects. In *Computational Intelligence in Internet of Agricultural Things* (pp. 171–192). Cham: Springer Nature Switzerland.

Elseidi, M. (2025). STR-NBEATS: a novel hybrid framework integrating time series decomposition with deep learning for enhanced temperature forecasting. *Modeling Earth Systems and Environment, 11*(4), 1–14.

Fister, D., Pérez-Aracil, J., Peláez-Rodríguez, C., Del Ser, J., & Salcedo-Sanz, S. (2023). Accurate long-term air temperature prediction with machine learning models and data reduction techniques. *Applied Soft Computing, 136*, 110118.

Franzke, C. L., & Torelló i Sentelles, H. (2020). Risk of extreme high fatalities due to weather and climate hazards and its connection to large-scale climate variability. *Climatic Change, 162*(2), 507–525.

Gong, B., Langguth, M., Ji, Y., Mozaffari, A., Stadtler, S., Mache, K., & Schultz, M. G. (2022). Temperature forecasting by deep learning methods. *Geoscientific Model Development, 15*(23), 8931–8956.

Huang, J., Xu, Y., Wang, Q., Wang, Q. C., Liang, X., Wang, F., ... & Fei, A. (2025). Foundation models and intelligent decision-making: Progress, challenges, and perspectives. *The Innovation*.

Islam, S., Karipot, A., Bhawar, R., Sinha, P., Kedia, S., & Khare, M. (2024). Urban heat island effect in India: a review of current status, impact and mitigation strategies. *Discover Cities, 1*(1), 1–28.

Javaid, M., Haleem, A., Khan, I. H., & Suman, R. (2023). Understanding the potential applications of Artificial Intelligence in Agriculture Sector. *Advanced Agrochem, 2*(1), 15–30.

Kumar, A., Ray, T., & Mohanasundari, T. (2024). Exploring Climatic Dynamics in Madhya Pradesh, India Utilizing Long-Term Gridded Data (1951–2021): An Integrated Statistical and GIS Modules. In *Integrated Management of Water Resources in India: A Computational Approach* (pp. 3–21). Cham: Springer Nature Switzerland.

Li, F., Diop, S., Hirwa, H., Maesho, S., Ning, X., Tian, C., ... & Chen, G. (2024). Dryland Social-Ecological Systems in Africa. In *Dryland Social-Ecological Systems in Changing Environments* (pp. 273–323). Singapore: Springer Nature Singapore.

McDonald, R. I., Biswas, T., Chakraborty, T. C., Kroeger, T., Cook-Patton, S. C., & Fargione, J. E. (2024). Current inequality and future potential of US urban tree cover for reducing heat-related health impacts. *npj Urban Sustainability, 4*(1), 18.

McGregor, G. (2024). Heatwave Responses: Early Warning Systems. In *Heatwaves: Causes, Consequences and Responses* (pp. 549–599). Cham: Springer International Publishing.

National Oceanic and Atmospheric Administration. (2023). U.S. climate data and summaries. https://www.noaa.gov/climate

Pascal, M., Lagarrigue, R., Tabai, A., Bonmarin, I., Camail, S., Laaidi, K., ... & Denys, S. (2021). Evolving heat waves characteristics challenge heat warning systems and prevention plans. *International Journal of Biometeorology, 65*, 1683–1694.

Pujahari, R. M., Yadav, S. P., & Khan, R. (2022). Intelligent farming system through weather forecast support and crop production. In *Application of Machine Learning in Agriculture* (pp. 113–130). Academic Press.

Rakhee, Hoda, M. N., & Bansal, S. (2024). Seasonal temperature forecasting using genetically tuned artificial neural network. *International Journal of Information Technology, 16*(1), 315–319.

Taherdoost, H. (2023). Deep learning and neural networks: Decision-making implications. *Symmetry, 15*(9), 1723.

Uluocak, I., & Bilgili, M. (2024). Daily air temperature forecasting using LSTM-CNN and GRU-CNN models. *Acta Geophysica, 72*(3), 2107–2126.

U.S. Census Bureau. (2023). County population totals and components of change: 2020–2023. https://www.census.gov/data/tables/time-series/demo/popest/2020s-counties-total.html

Vaidyanathan, A., Malilay, J., Schramm, P., & Saha, S. (2004). MMWR-Heat-Related Deaths—United States, 2004–2018.

Waqar, A. (2024). Intelligent decision support systems in construction engineering: An artificial intelligence and machine learning approaches. *Expert Systems with Applications, 249*, 123503.

Wang, A., Dai, Y., Zhang, M., & Chen, E. (2025). Exploring the cooling intensity of green cover on urban heat island: A case study of nine main urban districts in Chongqing. *Sustainable Cities and Society, 124*, 106299.

Wang, H., Ma, X., Cui, M., Dai, Y., Ye, X., Lv, X., & Wang, Y. (2023, November). Application of the Informer Long-Term Sequence Model in Agricultural Temperature Prediction. In *2023 China Automation Congress (CAC)* (pp. 7122–7127). IEEE.

Zhang, Z., Zhang, Q., Chen, B., Yu, Y., Wang, T., Xu, N., ... & Qian, H. (2024). Global biogeography of microbes driving ocean ecological status under climate change. *Nature Communications, 15*(1), 4657.